Key Engineering Materials Vols. 309-311 (2006) pp. 53-56
online at http://www.scientific.net

Formation of c-Axis Aligned Hydroxyapatite Sheet by Simultaneous Imposition of High Magnetic Field and Mold Rotation During Slip Casting Process

Jun Akiyama[1,a], Masami Hashimoto[2,b], Hiroaki Takadama[2,c], Fukue Nagata[3,d], Yoshiyuki Yokogawa[3,e], Kensuke Sassa[1,f], Kazuhiko Iwai[1,g] and Shigeo Asai[1,h]

[1]Department of Materials, Physics and Energy Engineering, Nagoya University, Nagoya 464-8603, Japan

[2]Japan Fine Ceramics Center, Nagoya 456-8587, Japan

[3]National Institute of Advanced Industrial Science and Technology, Nagoya 463-8560, Japan

[a]h052101d@mbox.nagoya-u.ac.jp, [b]masami@jfcc.or.jp, [c]takadama@jfcc.or.jp, [d]f.nagata@aist.go.jp, [e]y-yokogawa@aist.go.jp, [f]sassa@nagoya-u.jp, [g]d42859a@cc.nagoya-u.ac.jp, [h]c42538a@nucc.cc.nagoya-u.ac.jp

Keywords: Hydroxyapatite, Crystal alignment, High magnetic field, Mold rotation

Abstract. A high magnetic field is a useful tool to control the crystal alignment of non-magnetic materials such as ceramics and polymers. In the case of Hydroxyapatite crystal, the a,b-axis is aligned parallel to the direction of an imposed magnetic field. This fact implies that the alignment of the c-axis is not controllable only using a high static magnetic field due to the freedom of the c-axis in a plane perpendicular to a magnetic field direction. In this study, a high static magnetic field and mold rotation was simultaneously so applied during a slip casting process as to align the c-axis of HAp poly crystals.

Introduction

Hydroxyapatite (HAp), which has been widely applied as biomaterials and adsorbents of protein, shows anisotropic adsorbing characteristics due to a hexagonal crystal structure. For example, the c-plane of HAp is an adsorption site for amino acids in proteins and for sodium ions in buffer solutions, where a phosphoric acid is the main occupant in the crystal plane. On the other hand, the a,b-plane is favored adsorption sites for carboxyl groups in proteins, and for phosphoric acids in buffer solutions, because calcium is the main occupant in the crystal plane[1,2]. Therefore, the crystal alignment of HAp creates a new function relating with bioactivity and sorbability. Thus, the crystal alignment has been conducted using various methods, such as a slip casting under a high magnetic field[3,4], a tape casting and so on. However, it is not easy to produce a sample in which the c-axis of HAp crystals is highly aligned. In this study, a high static magnetic field and mold rotation during a slip casting were simultaneously so imposed as to get the high c-axis alignment of HAp crystals.

Experimental

The experimental apparatus is shown in Figure.1. A slurry containing HAp particles (Taihei Chemical Co., mean diameter: 2μm) and distilled water was mixed with a deflocculant, and mechanically ground for 4hrs to decompose agglomerated particles into single crystals. The slurry was poured into a mold with an inside diameter of 22mm and a capacity of 1500mm^3 made of gypsum, and the mold was put on a rotating platform set in a bore of a super conducting magnet for a slip casting. In this experiment, there are two operational variables: horizontally imposed high magnetic field of 10T and mold rotation of 0.3rad/s (Table 1). After the slip casting, the samples were dried in air over 24hrs without magnetic field and sintered at 1423K for 2hrs in atmosphere in an electric furnace. Finally the samples were examined by X-ray diffraction (XRD) and SEM observation. To evaluate the degree of crystal alignment in the samples, an intensity ratio which is defined as the ratio of (002) (corresponding to the c-plane) to (211) (the main peak of the diffraction of HAp powder) was calculated from the XRD patterns.

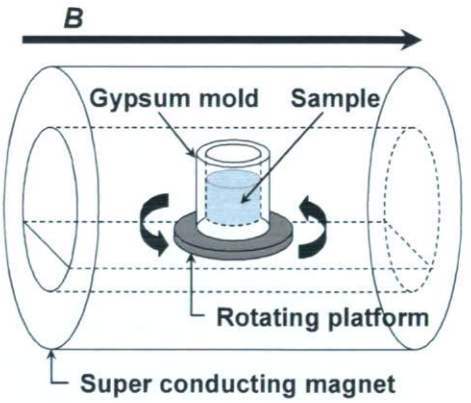

Fig.1 Experimental apparatus

Table 1 Experimental conditions and results

Sample ID	Magnetic Field [T]	Rotating velocity [rad/s]	Intensity ratio of (002) to (211)
1	0	0	0.36
2	0	0.3	0.32
3	10	0	0.71
4	10	0.3	53.0

Results and Discussion

The XRD patterns of the samples obtained under the different experimental conditions and their intensity ratio are shown in Fig.2 and Table 1. The diffraction patterns of the samples without the imposition of magnetic field and with or without mold rotation are shown in Fig.2-(1) and (2). These diffraction intensities of each peak are almost same as the powder diffraction of JCPDS card #9-432. The intensity ratio for the sample without magnetic field and without mold rotation is 0.36, while that without magnetic field and with mold rotation is 0.32. That is, no obvious crystal alignment was observed in the samples treated without magnetic field. The XRD pattern of the sample cast under the 10T magnetic field and without mold rotation is shown in Fig.2-(3). The diffraction intensity of the c-plane such as (002) increases in comparison with those for the sample treated without magnetic field, while those of (210), (300) and (310), which are perpendicular to the c-plane, decrease, and the intensity ratio is 0.71. This result tells that the c-plane in the sample somewhat increases by only imposing the high magnetic field, though the

complete c-plane alignment has not been achieved. The XRD pattern for the sample with the magnetic field of 10T and mold rotation is shown in Fig.2-(4). Only (002) and (004) peaks corresponding to the c-plane appear and other ones have scarcely been seen. The intensity ratio drastically increases to 53. That is, most of HAp crystals in this sample aligned to the c-plane.

Figure 3 shows the SEM image of the sample without both magnetic field and mold rotation. The diameter of grains is about 1-3μm and each particle is spherical shape. Figure 4 shows the SEM images of the sample with magnetic field and mold rotation. On the upper surface, hexagonal shape of crystals are clearly observed as shown in Fig.4-(a), while plate-like or pillar-like shapes are mainly seen on the cross sectional plane of the same sample as shown in Fig.4-(b). From these two SEM images, it is understood that hexagonal grains of HAp uni-axially aligned in perpendicular to the upper surface.

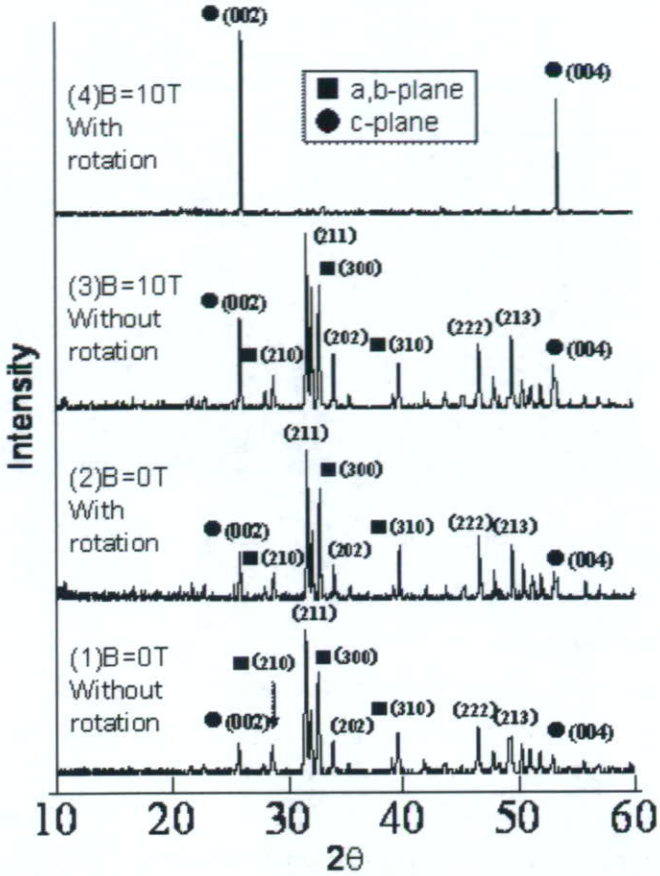

Fig.2 X-ray diffraction pattern of HAp under different experimental conditions.

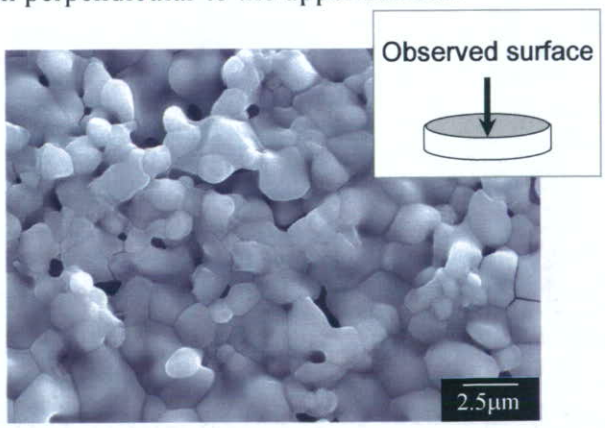

Fig.3 SEM image of the sample cast without magnetic field and mold rotation.

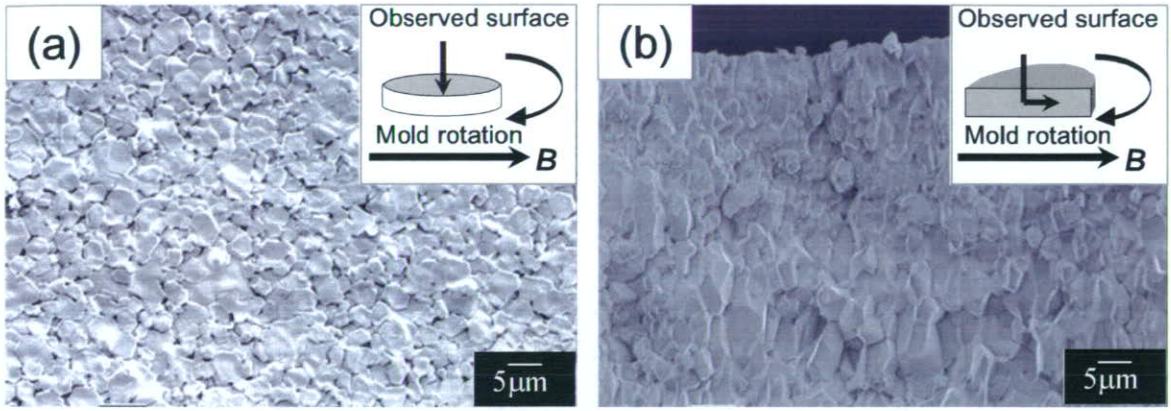

Fig.4 SEM images of the sample cast with magnetic field of 10T and mold rotation.
(a) surface, (b) cross-section

Conclusions

For producing of HAp crystals with the c-axis alignment, the high static magnetic field and mold rotation were applied during a slip casting process. From SEM observations and X-ray diffractions, it has been found that the c-axis of HAp crystals in the sample treated with magnetic field and mold rotation was highly aligned in comparison with those without magnetic field and with or without mold rotation. Therefore, this hybrid process encompassing the imposition of magnetic field and mold rotation in a slip casting is a useful tool for fabricating the c-axis alignment of HAp crystals.

Acknowledgement

This research was partially supported by the Ministry of Education, Culture, Sports, Science and Technology, Grant-in-Aid for Exploratory Research, (No.16656209), "Creation of Nature-Guided Materials Processing" of the 21st Century COE Program and research support program of SEKISUI CHEMICAL Company.

References

[1]T.Kawasaki:J.of.Chromatography 151 (1978), p.95-112

[2]T.Kawasaki, M.Nimura and Y.Kobayashi: J.of.Chromatography 515 (1990), p.91-123

[3]K.Inoue, T.Marukawa, K.Sassa, Y.Yokogawa, Y.Sakka, M.Okido and S.Asai : Key Engineering Materials 240-242 (2003), p.513-516.

[4]K.Inoue, K.Sassa, Y.Yokogawa, Y.Sakka, M.Okido and S.Asai: Mater.Trans. 44 (2003), p.1133-1137

厚生労働科学研究費補助金

基礎研究成果の臨床応用推進研究事業

長寿命型人工関節の臨床応用推進に関する研究

総合研究報告書

第２分冊（2/2）

主任研究者　高取吉雄

平成２０（２００８）年　４月

Available online at www.sciencedirect.com
ScienceDirect
Biomaterials 28 (2007) 3121–3130
Biomaterials
www.elsevier.com/locate/biomaterials

High lubricious surface of cobalt–chromium–molybdenum alloy prepared by grafting poly(2-methacryloyloxyethyl phosphorylcholine)

Masayuki Kyomoto[a,b,*], Yasuhiko Iwasaki[c], Toru Moro[d], Tomohiro Konno[b], Fumiaki Miyaji[a], Hiroshi Kawaguchi[d], Yoshio Takatori[d], Kozo Nakamura[d], Kazuhiko Ishihara[b]

[a]*Research Division, Japan Medical Materials Corporation, Japan*
[b]*Department of Materials Engineering, School of Engineering and Center for NanoBio Integration, The University of Tokyo, Japan*
[c]*Institute of Biomaterials and Bioengineering, Tokyo Medical and Dental University, Japan*
[d]*Department of Orthopaedic Surgery, School of Medicine, The University of Tokyo, Japan*

Received 19 December 2006; accepted 9 March 2007
Available online 18 March 2007

Abstract

Osteolysis caused by wear particles from polyethylene in artificial hip joints is of great concern. Various bearing couple combinations, bearing material improvements, and surface modifications have been attempted to reduce such wear particles. With the aim of reducing the wear and developing a novel artificial hip-joint system, we created a highly lubricious metal-bearing material: A 2-methacryloyloxyethyl phosphorylcholine (MPC) polymer was grafted onto the surface of the cobalt–chromium–molybdenum (Co–Cr–Mo) alloy. For ensuring the long-term retention of poly(MPC) on the Co–Cr–Mo alloy, we used a 4-methacryloxyethyl trimellitate anhydride (4-META) intermediate layer and photo-induced graft polymerization technique to create a strong bonding between the Co–Cr–Mo substrate and the poly(MPC) chain via the 4-META layer. The Co–Cr–Mo alloy was pretreated with nitric acid and O_2 plasma to facilitate efficient interaction between the 4-META carboxyl group and the surface hydroxyl group on the Cr oxide passive layer of the Co–Cr–Mo alloy. After MPC grafting, the MPC unit peaks were clearly observed in the Fourier-transform infrared spectroscopy with attenuated total reflection (FT-IR/ATR) and X-ray photoelectron spectroscopy (XPS) spectra of the Co–Cr–Mo surface. Tribological studies with a pin-on-plate machine revealed that surface MPC grafting markedly lowered the friction coefficient. We concluded that the grafted poly(MPC) layer successfully provided high lubricity to the Co–Cr–Mo surface.

Keywords: Joint replacement; Cobalt alloy; Phosphorylcholine; Metal surface treatment

1. Introduction

The number and prevalence of primary and revision hip and knee joint replacements are substantially increasing worldwide every year [1]. This implies that the quality of artificial joints is becoming increasingly important. Most patients who receive an artificial joint experience a dramatic relief from pain and enjoy a rapid improvement in their quality of life. The most widely used bearing couple in artificial hip-joint systems is the combination of an ultra-high-molecular weight polyethylene (UHMWPE) acetabular component and a metal femoral component. The cobalt–chromium–molybdenum (Co–Cr–Mo) alloy is one of the most widely used metal-bearing materials in artificial joint systems. The Co–Cr–Mo alloy has good mechanical properties, castability, corrosion resistance, and wear resistance, whereas stainless-steel and titanium alloys have a disadvantage with regard to corrosion resistance and wear resistance, respectively.

In total hip arthroplasty (THA), osteolysis caused by the wear particles from UHMWPE has been recognized as a serious issue [2–4]. Efforts to decrease these particles have focused on bearing material improvement and the use of

*Corresponding author. Uemura Nissei Bldg. 9F, 3-3-31 Miyahara, Yodogawa-ku, Osaka 532-0003 Japan. Tel.: +81 6 6350 1014; fax: +81 6 6350 5752.
E-mail address: kyomotom@jmmc.jp (M. Kyomoto).

0142-9612/$ - see front matter © 2007 Elsevier Ltd. All rights reserved.
doi:10.1016/j.biomaterials.2007.03.010

combinations other than metal-on-UHMWPE [5–7]. Recently, a metal-on-metal-type artificial hip-joint system consisting of Co–Cr–Mo acetabular and femoral components has been studied [8,9]. The advantages of the Co–Cr–Mo/Co–Cr–Mo bearings are the absence of the generation of UHMWPE wear debris and decreased wear as compared to that in the case of the Co–Cr–Mo/UHMWPE bearings [10,11]. However, even in the Co–Cr–Mo/Co–Cr–Mo bearings, aseptic loosening induced by wear particles and metallosis remain as serious issues in revision surgeries [12,13]. In addition to metallosis, electrochemical corrosion and carcinogenesis occurring due to the dissemination of wear particles to the other parts of the body have been reported [14].

To reduce such wear particles, improvements in the bearing materials and surface modifications of the Co–Cr–Mo alloy have been attempted [15,16]. Surface coating may reduce the UHMWPE wear without compromising the bulk mechanical properties of the implant materials. Various "hardening treatments" on metal-bearing surfaces, such as diamond-like carbon coating, titanium nitride coating, and ion implantation have been attempted [17–19]. Although these surface modifications may improve the THA survivorship, the limited THA longevity imposes restrictions for its application in younger patients. Consequently, the possibility of replacing the femoral head alone, in either solid or articular surface replacement form, during revision surgeries of metal-on-metal THA remains an attractive feature of such implants. However, the Co–Cr–Mo alloy or the hardening-treated Co–Cr–Mo alloy may induce damage to the cartilaginous tissue.

On the other hand, previous studies reported that highly lubricious hydrogel polymer used as an artificial cartilage did not damage against the cartilaginous tissue [20,21]. We have recently developed a highly lubricious artificial hip-joint system by a "mild treatment" with soft materials. In this treatment, poly(2-methacryloyloxyethyl phosphorylcholine (MPC)) was grafted onto the surface of CLPE (CLPE-*g*-MPC) [22–24]. MPC is a methacrylate monomer with a phospholipid polar group in a side chain and is used to prepare novel polymer biomaterials, as designed by Ishihara et al. [25] who were inspired by the neutral phospholipids of cell membranes. Many polymers containing the MPC unit are widely used as biomaterials [26–33]. Moreover, various medical devices have already been developed using poly(MPC) and are being used clinically. The efficacy of MPC polymer as a biomaterial has been well verified [34–36]. Based on the biocompatibility and hydrophilicity of poly(MPC), we have been developing new artificial joints with highly lubricious bearing surfaces that are formed by photo-induced radical graft polymerization.

In this study, we synthesized a highly lubricious metal-bearing material in which the MPC polymer was grafted onto the surface of the Co–Cr–Mo alloy (Co–Cr–Mo-*g*-MPC) for developing a novel artificial hip-joint system—artificial femoral head and metal-on-metal (Co–Cr–Mo/Co–Cr–Mo) type—for THA. We also investigated the surface structure and tribological properties of Co–Cr–Mo-*g*-MPC.

2. Materials and methods

2.1. Co–Cr–Mo alloy substrate and pretreatments

The Co–Cr–Mo alloy was supplied by Yoneda Advanced Casting Co., Ltd (Takaoka, Japan). The chemical composition of the Co–Cr–Mo alloy used in this study is listed in Table 1. This alloy was manufactured according to the ASTM F75 standard specification for Co–28Cr–6Mo alloy [37]. The Co–Cr–Mo samples were polished so that the average surface roughness ranged between 0.01 and 0.02 μm.

The polished Co–Cr–Mo samples were washed with acetone, and then immersed in 35vol% nitric acid at room temperature for 35 min according to the ASTM F86-04 standard [38]. This treatment provides passivation by surface oxidation and can dissolve certain foreign materials that may remain from the previous procedure. Moreover, a previous study reported that the Cr concentration of dry-polished stainless steel was lower at the surface than in the bulk [39]. We therefore treated the surface with nitric acid with the aim of increasing the Cr concentration by "re-surfacing."

After the nitric acid treatment, the Co–Cr–Mo samples were irradiated with O_2 plasma at 500-W high-frequency output and 150 mL/min O_2 gas flow for 5 min by using O_2 plasma etcher (PR500, Yamato Scientific Co., Ltd., Tokyo, Japan). The O_2 plasma treatment increased the thickness of the surface oxide layer.

2.2. 4-Methacryloxyethyl trimellitate anhydride coating on Co–Cr–Mo alloy and MPC graft polymerization

4-Methacryloxyethyl trimellitate anhydride (4-META) and acetone were purchased from Wako Pure Chemical Industries, Ltd. (Osaka, Japan). The previous studies suggested that 4-META and methacrylates were applicable as photocurable bonding liners that can bind a resin composite to a metal substrate [40–42]. MPC was synthesized industrially by using the method developed by Ishihara et al. [25] and was supplied by AI Bio-Chips Co., Ltd. (Tokyo, Japan). 2-Hydroxy-l-[4-(hydroxyethoxy)phenyl]-2-methyl-lpropanone (DAROCUR® 2959, D2959) was purchased from Ciba Specialty Chemicals Holding Inc. (Basel, Switzerland). D2959 is a highly efficient radical photoinitiator for ultraviolet (UV) curing of the systems containing unsaturated monomers and prepolymers. It is particularly well known as a cytocompatible UV photoinitiator with UV intensities of $<6\,mW/cm^2$ that can perform polymerization for up to 10 min with a UV light of 365 nm [43].

The synthesis of Co–Cr–Mo-*g*-MPC is schematically illustrated in Fig. 1. The various pretreated Co–Cr–Mo samples were coated with an

Table 1
Chemical composition (%) of the Co–Cr–Mo alloy

Cr	Mo	C	Ni	Fe	Si	Mn	Al	Co
28.61	5.96	0.03	0.02	0.03	0.54	0.40	0.02	Bal.

acetone solution containing 10mass% 4-META by using a spin coater (K-359 S-1, Kyowariken Inc., Tokyo, Japan) and then dried in the dark at 40 °C for 3 h to remove the acetone. MPC and D2959 were dissolved in degassed ethanol to a concentration of 2mass% and 0.1mass%, respectively. The Co–Cr–Mo samples coated with 4-META after various pretreatments were immersed in the MPC–ethanol solution containing D2959. Photo-induced graft polymerization on the Co–Cr–Mo surface was carried out using UV irradiation (UVL-400HA ultra-high-pressure mercury lamp, Riko-Kagaku Sangyo Co., Ltd., Finabashi, Japan) with an intensity of 5 mW/cm^2 at 60 °C for 10 min with a Toshiba D-35 filter to allow the passage of UV light of only 350 ± 50 nm wavelength. After the polymerization, the Co–Cr–Mo-*g*-MPC samples were removed from the solution, washed with ethanol, and dried at room temperature.

2.3. MPC graft polymerization on cross-linked polyethylene

Compression-molded UHMWPE (GUR1020 resin, Poly Hi Solidur Inc., IN, USA) bar stock was gamma irradiated at 50 kGy in N_2 gas and annealed at 120 °C in N_2 gas for cross-linking. After cooling, the cross-linked polyethylene (CLPE) specimens were machined from this bar stock.

MPC grafting onto the CLPE surface was performed as described in previous studies [23,24]. They were immersed in an acetone solution containing 10 mg/mL benzophenone for 30 s and then dried in the dark at room temperature to remove the acetone. MPC was dissolved in degassed pure water to a concentration of 0.5 mol/L. The benzophenone-coated CLPE samples were immersed in the aqueous MPC solution. Photo-induced graft polymerization on the CLPE surface was carried out using UV irradiation with an intensity of 5 mW/cm^2 at 60 °C for 90 min. After the polymerization, the CLPE-*g*-MPC samples were removed from the solution, washed with pure water and ethanol, and dried.

2.4. Surface analysis by Fourier-transform infrared spectroscopy, X-ray photoelectron spectroscopy, and water-contact angle measurement

The functional group vibrations of the Co–Cr–Mo alloy surfaces before and after the MPC grafting were examined by Fourier-transform infrared (FT-IR) spectroscopy with attenuated total reflection (ATR) equipment. The FT-IR/ATR spectra were obtained using an FT-IR analyzer (FT/IR615, JASCO Co. Ltd., Tokyo, Japan) for 32 scans (1.2 s/scan) over the range of 800–2000 cm^{-1} at a resolution of 4.0 cm^{-1}.

The surface elemental conditions of the Co–Cr–Mo alloy before and after the MPC grafting were analyzed using X-ray photoelectron spectroscopy (XPS). The XPS spectra were obtained using an XPS spectrophotometer (AXIS-HSi165, Kratos Analytical Ltd., UK) equipped with a 15-kV Mg-Kα radiation source at the anode. The take-off angle of the photoelectrons was maintained at 90°. Five scans (approximately 260–425 s/scan depending on the atomic signal strength) were taken for each sample.

The static water contact angles on the Co–Cr–Mo surfaces that were subjected to different types of pretreatments before and after the MPC grafting were measured using the sessile drop method with an optical bench-type contact angle goniometer (Model DM300, Kyowa Interface Science Co., Ltd., Saitama, Japan). Drops of purified water (1 μL) were deposited on the Co–Cr–Mo-*g*-MPC surface, and the contact angles were directly measured with a microscope after 60 s of dropping, according to the ISO 15989 standard [44]. Measurements were repeated six times for each sample, and the average values were considered as the contact angles.

2.5. Surface observation by fluorescence microscopy

We used rhodamine 6G (Wako Pure Chemical Industries, Ltd., Osaka, Japan) that can be applied simply and rapidly to a polymer coating and

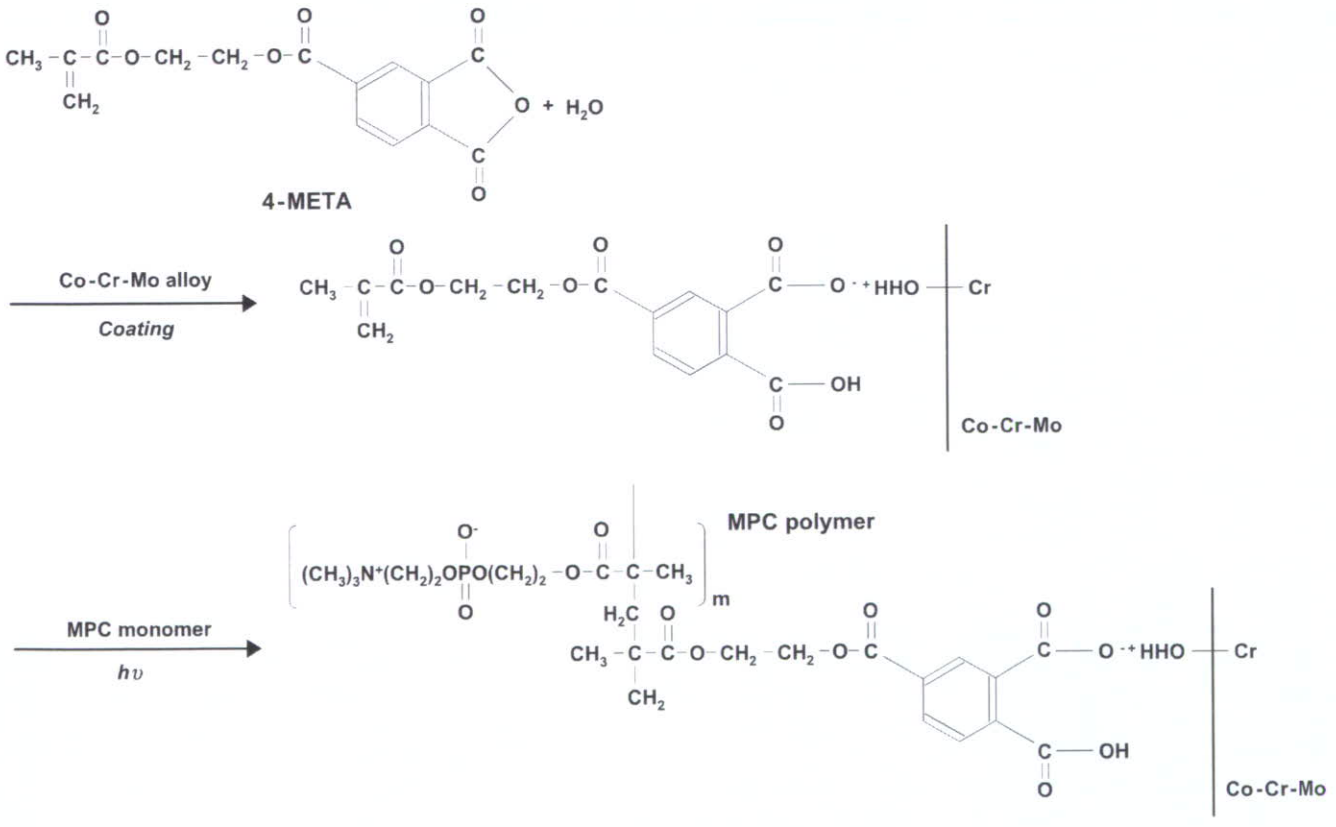

Fig. 1. Scheme for the synthesis of Co–Cr–Mo-*g*-MPC.

imaged using fluorescence microscopy (FM). Wang et al. [45] found that rhodamine 6G effectively stains poly(MPC) that possesses great structural similarity to lipids. This simple staining technique enables the evaluation of the coated area by FM.

An aqueous solution of 200 mass ppm rhodamine 6G was used for all the staining experiments. All the samples were stained by following a two-step procedure: (1) The samples were immersed in the rhodamine 6G solution for 30 s and then removed. (2) Next, they were washed two times consecutively in distilled water for 30 s and then dried.

A fluorescence microscope (Axioskop 2 Plus, Carl Zeiss AG, Oberkochen, Germany) was used for FM imaging and examination of all samples. Pseudo-color images were obtained using a CCD camera (VB-7010, Keyence Co., Osaka, Japan) and imaging software (VH analyzer 2.51, Keyence Co., Osaka, Japan). Lenses with $\times 10$ magnification and appropriate exposure time (approximately 1/10 s) were employed to obtain best image quality of the various samples.

It is known that most fluorescent dyes undergo a process called photobleaching under normal imaging conditions, with subsequent deterioration during fluorescence [45]. In general, the fluorescence intensity decreases with time during imaging [45]. In the present study, the Co–Cr–Mo-*g*-MPC samples were stained with rhodamine 6G, and they were illuminated within 5 min of staining. The time required for appropriate exposure was within 1–2 min. It was therefore assumed that the effect of photobleaching of rhodamine 6G was not very significant under these experimental conditions.

2.6. Friction test

The friction coefficients between the pins fabricated from various materials and the untreated Co–Cr–Mo ($n = 2$) or Co–Cr–Mo-*g*-MPC (pretreated with nitric acid and O_2 plasma, $n = 3$) plates were measured using a custom-made pin-on-plate machine [46]. Each pin was a cylinder measuring 5 mm in height and 9 mm in diameter. Friction tests were carried out at a temperature of 37 °C, a contact stress of 2.4 MPa, and a swing distance of 25 mm with a frequency of 1 Hz [47]. The lubricant used was a mixture of 27vol% bovine serum, 20 mM/L of ethylene diamine tetraacetic acid (EDTA), and 0.2mass% sodium azide [48]. The friction tests were performed up to maximum 5.0×10^4 cycles (preliminary test, $n = 1$), and the lubricant was not changed during the tests.

3. Results

Fig. 2 shows the FT-IR/ATR spectra of the untreated Co–Cr–Mo sample and the nitric acid- and O_2 plasma-pretreated Co–Cr–Mo-*g*-MPC sample. Absorption peaks were not observed for the Co–Cr–Mo sample before the MPC grafting and for either the nitric acid- or O_2 plasma-pretreated Co–Cr–Mo-*g*-MPC samples (data not shown). In contrast, new absorption peaks were observed only for the Co–Cr–Mo-*g*-MPC samples pretreated with both nitric acid and O_2 plasma. The peaks at 1720, 1550, and 1460 cm^{-1} are attributed to the aromatic ring C=O and -CH_2- in the 4-META and MPC graft polymer. The peaks at 1080 and 970 cm^{-1} are due to the phosphate group in the MPC unit [25].

Table 2 summarizes the elemental compositions of the Co–Cr–Mo surfaces that were subjected to the different types of pretreatments. After the nitric acid pretreatment, the O_2 and Co compositions decreased and the Cr and Mo compositions increased. After O_2 plasma pretreatment, the O_2 composition increased to approximately 53% due to the formation of the surface oxide layer. After the combined nitric acid and O_2 plasma pretreatment, the compositions of O_2, Co, and Cr were higher than those before the pretreatment.

The XPS spectra of the binding energy region of the Co_{2p}, Cr_{2p}, and Mo_{3d} electrons obtained from the nitric acid- and O_2 plasma-pretreated Co–Cr–Mo sample before and after the 4-META coating are shown in Fig. 3. Prior to the 4-META coating, the Co oxide (Co^{2+}), Cr oxide (Cr^{3+}), and Mo oxide (Mo^{4+} and Mo^{6+}) peaks were observed in the Co_{2p}, Cr_{2p}, and Mo_{3d} spectra, respectively. After the 4-META coating, Co_{2p} and Mo_{3d} were depleted but Cr_{2p} was almost unchanged.

Fig. 4 shows the XPS spectra (N_{1s} and P_{2p}) of the untreated Co–Cr–Mo sample and the nitric acid- and O_2 plasma-pretreated Co–Cr–Mo-*g*-MPC sample. In both N_{1s} and P_{2p} spectra, the peaks appeared only for Co–Cr–Mo-*g*-MPC. The peaks at 403 and 134 eV were assigned to the $-N^+(CH_3)_3$ and phosphate groups, respectively. These peaks are the characteristic of the phosphorylcholine present in the MPC units.

Table 3 summarizes the elemental compositions of the Co–Cr–Mo-*g*-MPC surfaces that were subjected to different types of pretreatments. The surface nitrogen (N) and phosphorous (P) compositions in the Co–Cr–Mo-*g*-MPC samples were higher than those in the untreated Co–Cr–Mo samples. It should be noted that in the Co–Cr–Mo-*g*-MPC samples pretreated with both nitric acid and O_2 plasma, the measured N and P compositions increased to 3.0 and 2.9, respectively, and the Co, Cr, and Mo from the Co–Cr–Mo substrate were not detected.

Fig. 5 shows the static water contact angle on the Co–Cr–Mo surfaces subjected to different types of pretreatments before and after the MPC grafting. The

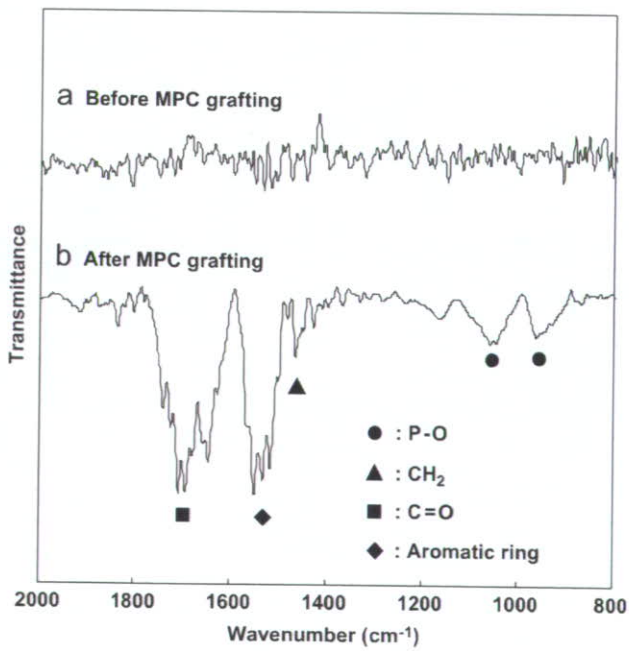

Fig. 2. FT-IR/ATR spectra of the nitric acid- and O_2 plasma-pretreated Co–Cr–Mo sample (a) before and (b) after MPC grafting.

static water contact angle on the Co–Cr–Mo surface before the MPC grafting was approximately 70°–90°; however, among the three differently pretreated surfaces, the nitric acid- and O_2 plasma-pretreated Co–Cr–Mo-*g*-MPC surface showed the lowest angle. The static water contact angle on the nitric acid- and O_2 plasma-pretreated Co–Cr–Mo-*g*-MPC surface was as low as 15°. On the other hand, compared to the angle on the untreated Co–Cr–Mo surface, the angle on the only nitric acid-pretreated Co–Cr–Mo-*g*-MPC surface was almost unchanged (approximately 65°) and that on the only O_2 plasma-pretreated Co–Cr–Mo-*g*-MPC surface was slightly decreased to 45°.

Fig. 6 shows the FM images of the untreated Co–Cr–Mo surface and the nitric acid- and O_2 plasma-pretreated Co–Cr–Mo-*g*-MPC surface. On the Co–Cr–Mo-*g*-MPC surface, rhodamine 6G stained poly(MPC) selectively (Fig. 6(b)). This resulted in a large contrast in the fluorescence intensity between the MPC-grafted layer (green–yellow) and the non-grafted substrates (blue) (Fig. 6(d)). The poly(MPC) layer stained with rhodamine 6G was more clearly visible but the staining was not uniform. It therefore indicates that the grafting of the poly(MPC) layer on the Co–Cr–Mo surface is not uniform. On the untreated Co–Cr–Mo surface, such a contrast was not observed (Fig. 6(a) and (c)).

Fig. 7 shows the friction coefficients of the sliding couples, namely, Co–Cr–Mo-*g*-MPC, CLPE, CLPE-*g*-MPC, and untreated Co–Cr–Mo pins sliding against the Co–Cr–Mo-*g*-MPC and untreated Co–Cr–Mo plates. The Co–Cr–Mo/Co–Cr–Mo couple showed a high friction coefficient of approximately 0.24 in the initial 10 cycles; the value increased gradually and reached approximately 0.38 after 5.0×10^4 cycles. The CLPE/Co–Cr–Mo-*g*-MPC and Co–Cr–Mo/Co–Cr–Mo-*g*-MPC couples showed a lower friction coefficient than the CLPE/untreated Co–Cr–Mo and Co–Cr–Mo/untreated Co–Cr–Mo couples, respectively. The CLPE/Co–Cr–Mo-*g*-MPC couple showed the lowest friction coefficient of approximately 0.05, and this value was almost steady during the experiment. In both CLPE-*g*-MPC/Co–Cr–Mo-*g*-MPC and Co–Cr–Mo-*g*-MPC/Co–Cr–Mo-*g*-MPC couples, the poly(MPC) layer sliding against the MPC polymer layer showed almost the same friction coefficient of approximately 0.12 up to the initial 100 cycles. After 5.0×10^4 cycles, the friction coefficients of the Co–Cr–Mo/Co–Cr–Mo-*g*-MPC and Co–Cr–Mo-*g*-MPC/Co–Cr–Mo-*g*-MPC couples increased, whereas that of the CLPE-*g*-MPC/Co–Cr–Mo-*g*-MPC couple decreased.

4. Discussion

In this study, with the aim of reducing wear, we synthesized a high lubricious Co–Cr–Mo alloy surface by poly(MPC) grafting for its application in artificial joints. To ensure the in vivo long-term retention of this

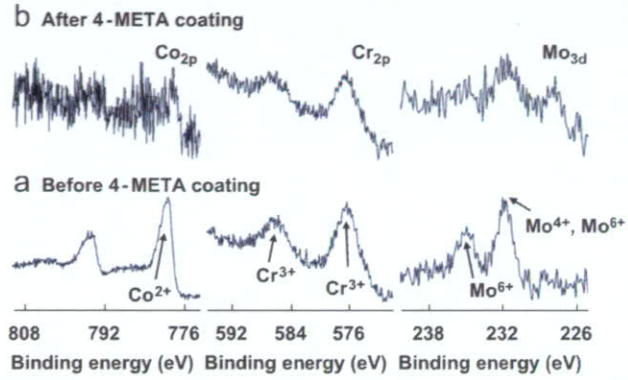

Fig. 3. XPS spectra of the binding energy region of the Co_{2p}, Cr_{2p}, and Mo_{3d} electrons from the nitric acid- and O_2 plasma-pretreated Co–Cr–Mo samples (a) before and (b) after the 4-META coating.

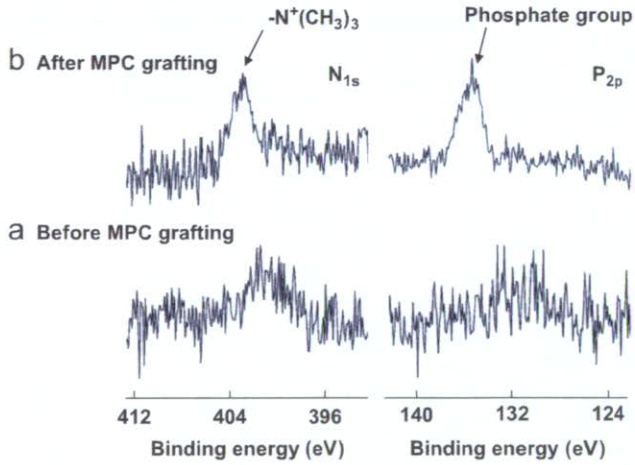

Fig. 4. XPS spectra (N_{1s} and P_{2p}) of the (a) untreated Co–Cr–Mo and (b) nitric acid- and O_2 plasma-pretreated Co–Cr–Mo-*g*-MPC samples.

Table 2
Surface elemental composition (%) of the pretreated Co–Cr–Mo alloy before MPC graft polymerization

Pretreatment	C_{1s}	O_{1s}	N_{1s}	P_{2p}	Co_{2p}	Cr_{2p}	Mo_{3d}
Untreated	44.2 (5.1)	39.3 (2.8)	0.6 (0.2)	0.0 (0.0)	10.5 (2.5)	4.5 (0.5)	1.0 (0.2)
Nitric acid	29.6 (3.8)	37.3 (1.6)	0.4 (0.8)	0.0 (0.0)	9.4 (0.7)	21.3 (2.1)	2.1 (0.2)
O_2 plasma	13.9 (0.5)	53.5 (0.9)	0.0 (0.0)	0.0 (0.0)	30.5 (1.2)	1.8 (0.5)	0.3 (0.1)
Nitric acid + O_2 plasma	14.6 (1.3)	52.9 (2.7)	0.0 (0.0)	0.0 (0.0)	26.7 (1.5)	5.4 (0.2)	0.4 (0.0)

$n = 5$.
The standard deviations are shown in parentheses.

Table 3
Surface elemental composition (%) of the Co–Cr–Mo-*g*-MPC samples that were subjected to different types of pretreatments

Pretreatment	MPC treatment	C_{1s}	O_{1s}	N_{1s}	P_{2p}	Co_{2p}	Cr_{2p}	Mo_{3d}
Nitric acid + O_2 plasma	Untreated	14.6 (1.3)	52.9 (2.7)	0.0 (0.0)	0.0 (0.0)	26.7 (1.5)	5.4 (0.2)	0.4 (0.0)
Untreated	MPC treatment	52.3 (1.3)	35.3 (0.4)	0.3 (0.2)	0.9 (0.1)	4.8 (0.8)	5.6 (1.1)	0.8 (0.1)
Nitric acid	MPC treatment	52.1 (1.1)	36.2 (0.7)	0.4 (0.2)	1.6 (0.2)	3.4 (0.4)	5.7 (0.7)	0.7 (0.2)
O_2 plasma	MPC treatment	42.1 (1.1)	45.6 (1.1)	0.2 (0.2)	1.0 (0.1)	10.5 (0.7)	0.4 (0.5)	0.2 (0.1)
Nitric acid + O_2 plasma	MPC treatment	63.3 (0.6)	30.8 (0.7)	3.0 (0.2)	2.9 (0.1)	0.0 (0.0)	0.0 (0.0)	0.0 (0.0)
MPC polymer*	MPC treatment	57.9	31.6	5.3	5.3	—	—	—

$n = 5$.
*Theoretical elemental composition of MPC polymer. The standard deviations are shown in parentheses.

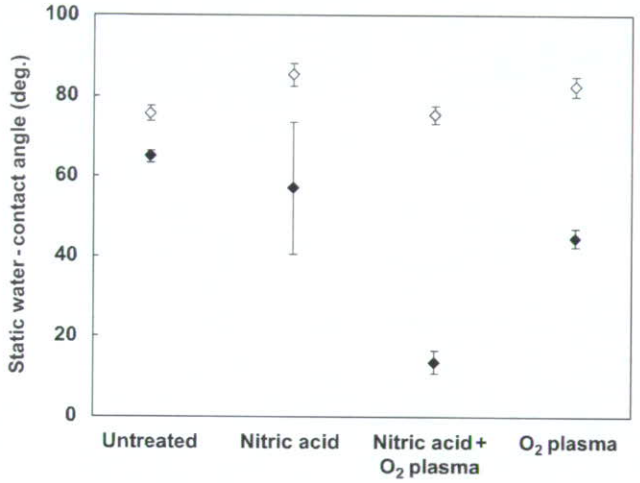

Fig. 5. Static water contact angle on the Co–Cr–Mo surfaces that were subjected to different types of pretreatments before and after the MPC grafting. Open marks, before MPC grafting; closed marks, after MPC grafting.

poly(MPC) graft on the Co–Cr–Mo alloy, we used the 4-META intermediate layer and the photo-induced radical graft polymerization technique to create a strong bonding between the Co–Cr–Mo substrate and the poly(MPC) chain via the 4-META layer. 4-META has already been known as a binder used in dental resin, and it can strongly bind resin to metal in dental implants [41,42]. Suzuki et al. [49] reported a strong evidence that the carboxylate anions were formed due to an ionic interaction between the carboxyl group of poly(carbonic acid) and the surface hydroxyl group on the oxide layer of stainless steel. Yamabe [50] reported that an ionic bond was formed between the carboxyl group and Cr on the surface of stainless steel. The various pretreatments performed in this study aimed at an efficient interaction between the carboxyl group of the 4-META layer and the surface hydroxyl group on the Cr oxide layer of the Co–Cr–Mo alloy.

As presented in Table 2, the surface Cr content in the Co–Cr–Mo alloy after the nitric acid pretreatment was higher than that of the untreated Co–Cr–Mo alloy. Seo and Sato [39] reported that a dry-polished stainless steel lacked in the surface Cr content. Accordingly, the as-polished Co–Cr–Mo alloy in this study may also lack the surface Cr content, and the surface etching by nitric acid treatment would have produced the Cr-rich surface layer.

Exposure of the Co–Cr–Mo alloy to O_2 plasma formed an oxide layer on the Co–Cr–Mo surface (Table 2 and Fig. 3(a)). The static water contact angle on the nitric acid-pretreated Co–Cr–Mo-*g*-MPC surface was higher than that on the nitric acid- and O_2 plasma-pretreated Co–Cr–Mo-*g*-MPC surface (Fig. 5). Additionally, the measured compositions of N and P in the only nitric acid-pretreated Co–Cr–Mo-*g*-MPC samples were lower than those in the nitric acid- and O_2 plasma-pretreated Co–Cr–Mo-*g*-MPC samples (Table 3). It was considered that washing with ethanol removed the 4-META-MPC graft copolymer (4-META-*co*-MPC) from the only nitric acid-pretreated Co–Cr–Mo surface because there was an inadequate ionic bonding between 4-META and the only nitric acid-pretreated Co–Cr–Mo surface without an oxide layer.

The peaks at 780, 236, and 232 eV in the XPS spectra were assigned to Co^{2+}, Mo^{4+}, and Mo^{6+}, respectively, as shown in Fig. 3. After the 4-META coating, these peaks disappeared from the Co–Cr–Mo surface. The peaks at 586 and 576 eV in the XPS spectra were assigned to Cr^{3+} (Fig. 3), indicating that Cr^{3+} persisted on the Co–Cr–Mo surface even after the 4-META coating. These results suggest that compared to other metallic oxides, Cr^{3+} predominantly binds to the carboxyl group of 4-META with a stronger ionic interaction [50]. This can be explained by the Lewis acid–base interaction model of a previous study [50]. It is assumed that the proton exchange between the carboxyl groups and active electrophilic metallic ions existing in the surface-hydrated oxide resulted in the formation of carboxylate anions; these carboxyl species that diffused into the hydrated oxide layer could easily undergo strong ionic interactions with the polar hydroxyl groups of hydrated Cr^{3+}. The binding between 4-META-*co*-MPC and the Co–Cr–Mo substrate might contribute to the stable polymer/metal interface.

Friction coefficients of various bearing couples in the previous studies are summarized in Table 4. In Fig. 7, the Co–Cr–Mo/Co–Cr–Mo couple showed a friction coefficient of approximately 0.24 as high as the previous studies. The CLPE/Co–Cr–Mo couple also showed a friction coefficient of approximately 0.09 as high as the previous studies. In contrast, it was confirmed that compared to the

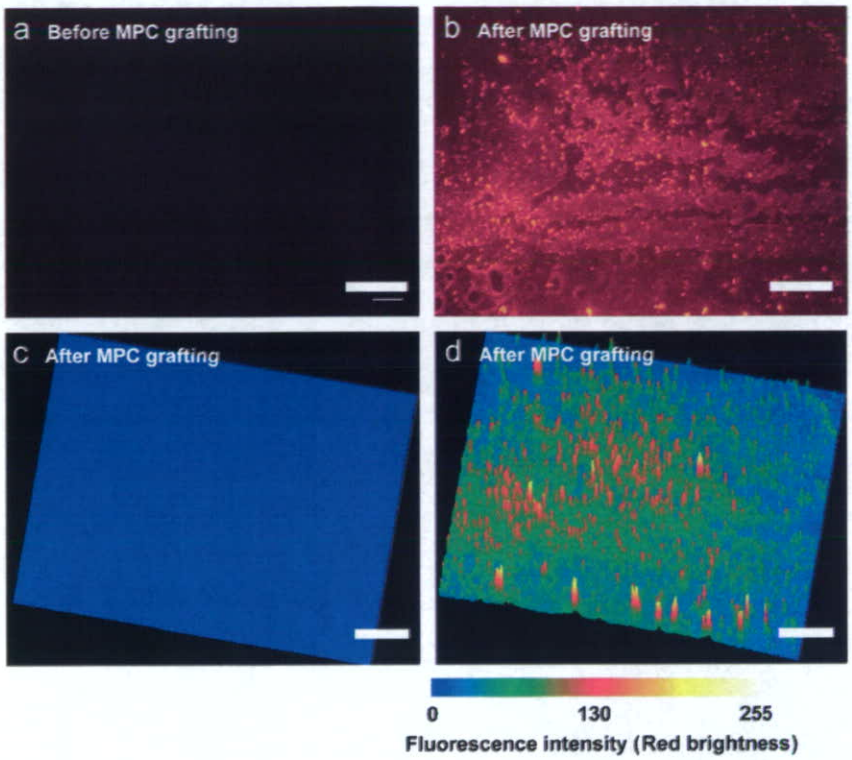

Fig. 6. FM images of (a), (c) the untreated Co–Cr–Mo and (b), (d) the nitric acid- and O_2 plasma-pretreated Co–Cr–Mo-*g*-MPC samples. (a and b) = FM images; (c and d) = color images from fluorescence intensity of the FM images (a and b). Bar = 200 μm. Color scale bar indicates fluorescence intensity (red brightness) for (c and d).

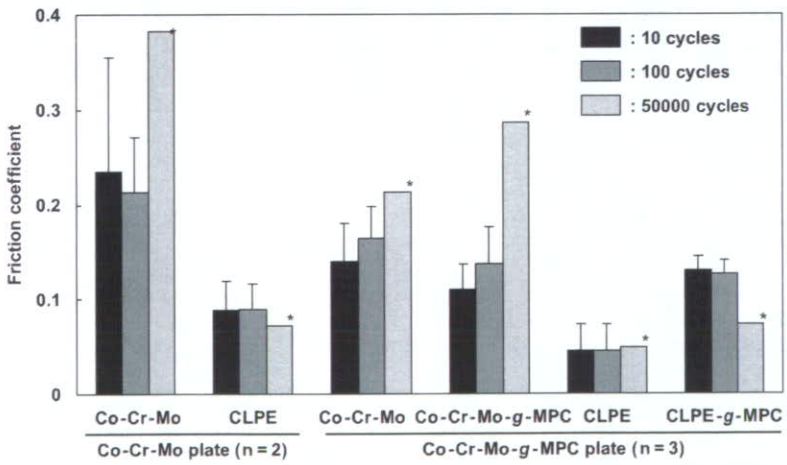

Fig. 7. Friction coefficients as a function of the test duration for the various types of pins sliding against the Co–Cr–Mo-*g*-MPC ($n = 3$) and untreated Co–Cr–Mo ($n = 2$) plates. *$n = 1$. Bars = standard deviations.

untreated Co–Cr–Mo surface, the Co–Cr–Mo-*g*-MPC (excluding the CLPE-*g*-MPC/Co–Cr–Mo-*g*-MPC-bearing couple) surface showed an extremely low friction coefficient. Since MPC is highly hydrophilic and poly(MPC) is water soluble, the water wettability of the Co–Cr–Mo-*g*-MPC surface was greater than that of the untreated Co–Cr–Mo surface, as shown in Fig. 5. Consequently, the grafted poly(MPC) layer successfully provided high lubricity to the Co–Cr–Mo surface (Fig. 7). The reduction in the friction may contribute to the improvement in the anti-wear properties [22]. From the viewpoint of tribological advantage, a highly lubricious metal-bearing material will enable the development of a novel biocompatible artificial hip-joint system.

Various factors such as the type of bearing material, surface roughness, homogeneity of the surface, and chemical composition affect the lubricity of artificial joints [54]. In the case of Co–Cr–Mo-*g*-MPC, the lubricity would

Table 4
Friction coefficients of various bearing couples in the previous studies

Bearing couple		Friction coefficient	References
Pin	Disc or plate		
Co–Cr–Mo	Co–Cr–Mo	0.19–0.27	[51]
UHMWPE	Co–Cr–Mo	0.05–0.09	[52]
UHMWPE	Co–Cr–Mo	0.05–0.09	[53]
Cartilage	Stainless steel	0.01–0.05	[55]
Cartilage	Cartilage	0.02	[56]

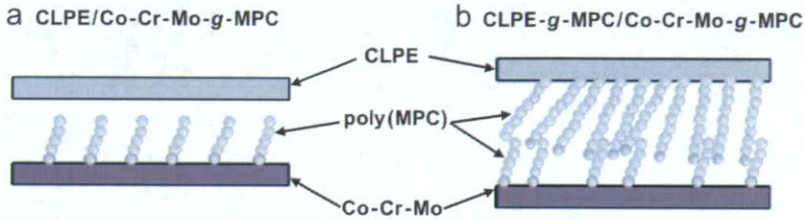

Fig. 8. Images of grafted non-grafted poly(MPC)/grafted poly(MPC) and poly(MPC)/grafted poly(MPC)-bearing interfaces.

change depending on the ambient in vitro and in vivo conditions. The bearing surface with poly(MPC) in artificial hip joints is assumed to have a structure similar to an artificial cell membrane. The Co–Cr–Mo-*g*-MPC/Co–Cr–Mo-*g*-MPC or CLPE-*g*-MPC/Co–Cr–Mo-*g*-MPC-bearing couples therefore mimic the natural joint cartilage in vivo. A friction coefficient of cartilage/SUS pin-on-plate was 0.01–0.05 [55], and that of cartilage/cartilage pin-on-plate was 0.02 [56], as shown in Table 4. In contrast, the Co–Cr–Mo-*g*-MPC/Co–Cr–Mo-*g*-MPC or CLPE-*g*-MPC/Co–Cr–Mo-*g*-MPC-bearing couples mimicking the natural joint, showed high friction (friction coefficient = 0.12) in this study. Images of grafted non-grafted poly(MPC)/grafted poly(MPC) and poly(MPC)/grafted poly(MPC)-bearing interfaces are shown in Fig. 8. The grafted poly(MPC)/non-grafted poly(MPC)-bearing interface in the CLPE/Co–Cr–Mo-*g*-MPC couple showed a low friction coefficient with the water wettability of poly(MPC) (Fig. 8(a)). The grafted poly(MPC)/grafted poly(MPC)-bearing interface in the CLPE-*g*-MPC/Co–Cr–Mo-*g*-MPC couple showed slightly higher friction than the grafted poly(MPC)/non-grafted poly(MPC)-bearing interface. The MPC graft polymer on Co–Cr–Mo might have low density because the polymerization method used was "grafting to" [57]. Fukuda et al. [58] reported that the friction was higher in a bearing couple with low-density polymer brushes than in a bearing couple with high-density polymer brushes. Therefore, it is assumed that a bearing couple with low-density poly(MPC) brushes may cause high friction with interpenetration as shown in Fig. 8(b) [59]. High-density poly(MPC) by "grafting from" might be possible to resist the interpenetration by its volume effects arising from chain mobility.

5. Conclusions

We created a highly lubricious metal-bearing material for its application as a novel artificial hip-joint system: The MPC polymer was grafted onto the surface of the Co–Cr–Mo alloy by employing the 4-META intermediate layer and using the photo-induced radical graft polymerization technique and the nitric acid and O_2 plasma pretreatments of the Co–Cr–Mo alloy. In conclusion, the grafted poly(MPC) layer successfully provided high lubricity to the Co–Cr–Mo surface. The grafted poly(MPC)/non-grafted poly(MPC)-bearing interface had a lower friction value than that of the grafted poly(MPC)/grafted poly(MPC) bearing interface.

References

[1] Kurtz S, Mowat F, Ong K, Chan N, Lau E, Halpern M. Prevalence of primary and revision total hip and knee arthroplasty in the United States from 1990 through 2002. J Bone Joint Surg Am 2005;87(7):1487–97.
[2] Harris WH. The problem is osteolysis. Clin Orthop 1995;311:46–53.
[3] Kobayashi A, Freeman MA, Bonfield W, Kadoya Y, Yamac T, Al-Saffar N, et al. Number of polyethylene particles and osteolysis in total joint replacements. A quantitative study using a tissue-digestion method. J Bone Joint Surg Br 1997;79(5):844–8.
[4] Sochart DH. Relationship of acetabular wear to osteolysis and loosening in total hip arthroplasty. Clin Orthop 1999;363:135–50.
[5] McKellop H, Shen FW, Lu B, Campbell P, Salovey R. Development of an extremely wear-resistant ultra high molecular weight polyethylene for total hip replacements. J Orthop Res 1999;17(2):157–67.
[6] Muratoglu OK, Bragdon CR, O'Connor DO, Jasty M, Harris WH. A novel method of crosslinking ultra-high-molecular-weight polyethylene to improve wear, reduce oxidation, and retain mechanical properties: recipient of the 1999 HAP Paul Award. J Arthroplasty 2001;16(2):149–60.

[7] Urban JA, Garvin KL, Boese CK, Bryson L, Pedersen DR, Callaghan JJ, et al. Ceramic-on-polyethylene bearing surfaces in total hip arthroplasty. Seventeen to twenty-one-year results. J Bone Joint Surg Am 2001;83(11):1688–94.
[8] St John KR, Zardiackas LD, Poggie RA. Wear evaluation of cobalt–chromium alloy for use in a metal-on-metal hip prosthesis. J Biomed Mater Res B Appl Biomater 2004;68(1):1–14.
[9] McMinn DJ, Daniel J, Pynsent PB, Pradhan C. Mini-incision resurfacing arthroplasty of hip through the posterior approach. Clin Orthop Relat Res 2005;441:91–8.
[10] Clarke IC, Good V, Williams P, Schroeder D, Anissian L, Stark A, et al. Ultra-low wear rates for rigid-on-rigid bearings in total hip replacements. Proc Inst Mech Eng [H] 2000;214(4):331–47.
[11] Fisher J, Hu XQ, Stewart TD, Williams S, Tipper JL, Ingham E, et al. Wear of surface engineered metal-on-metal hip prostheses. J Mater Sci Mater Med 2004;15(3):225–35.
[12] Keel JB, Kuster MS. Massive wear of an incompatible metal-on-metal articulation in total hip arthroplasty. J Arthroplasty 2004;19(5):638–42.
[13] Korovessis P, Petsinis G, Repanti M, Repantis T. Metallosis after contemporary metal-on-metal total hip arthroplasty. Five to nine-year follow-up. J Bone Joint Surg Am 2006;88(6):1183–91.
[14] Savarino L, Granchi D, Ciapetti G, Cenni E, Nardi Pantoli A, Rotini R, et al. Ion release in patients with metal-on-metal hip bearings in total joint replacement: a comparison with metal-on-polyethylene bearings. J Biomed Mater Res 2002;63(5):467–74.
[15] Dowson D, Hardaker C, Flett M, Isaac GH. A hip joint simulator study of the performance of metal-on-metal joints: Part I: the role of materials. J Arthroplasty 2004;19(8):118–23.
[16] Bowsher JG, Nevelos J, Williams PA, Shelton JC. 'Severe' wear challenge to 'as-cast' and 'double heat-treated' large-diameter metal-on-metal hip bearings. Proc Inst Mech Eng [H] 2006;220(2):135–43.
[17] Brizuela M, Garcia-Luis A, Viviente JL, Braceras I, Onate JI. Tribological study of lubricious DLC biocompatible coatings. J Mater Sci Mater Med 2002;13(12):1129–33.
[18] Gutmanas EY, Gotman I. PIRAC Ti nitride coated Ti-6Al-4V head against UHMWPE acetabular cup-hip wear simulator study. J Mater Sci Mater Med 2004;15(4):327–30.
[19] Bowsher JG, Hussain A, Williams P, Nevelos J, Shelton JC. Effect of ion implantation on the tribology of metal-on-metal hip prostheses. J Arthroplasty 2004;19(8):107–11.
[20] Oka M, Ushio K, Kumar P, Ikeuchi K, Hyon SH, Nakamura T, et al. Development of artificial articular cartilage. Proc Inst Mech Eng [H] 2000;214(1):59–68.
[21] Ushio K, Oka M, Hyon SH, Yura S, Toguchida J, Nakamura T. Partial hemiarthroplasty for the treatment of osteonecrosis of the femoral head. An experimental study in the dog. J Bone Joint Surg Br 2003;85(6):922–30.
[22] Moro T, Takatori Y, Ishihara K, Konno T, Takigawa Y, Matsushita T, et al. Surface grafting of artificial joints with a biocompatible polymer for preventing periprosthetic osteolysis. Nat Mater 2004;3:829–37.
[23] Kyomoto M, Moro T, Konno T, Takadama H, Yamawaki N, Kawaguchi H, et al. Enhanced wear resistance of modified cross-linked polyethylene by grafting with poly(2-methacryloyloxyethyl phosphorylcholine). J Biomed Mater Res A, forthcoming.
[24] Kyomoto M, Moro T, Konno T, Takadama H, Kawaguchi H, Takatori Y, et al. Effects of photo-induced graft polymerization of 2-methacryloyloxyethyl phosphorylcholine on physical properties of cross-linked polyethylene in artificial hip joints. J Mater Sci Mater Med, forthcoming.
[25] Ishihara K, Ueda T, Nakabayashi N. Preparation of phospholipid polymers and their properties as polymer hydrogel membranes. Polym J 1990;22(5):355–60.
[26] Ishihara K, Aragaki R, Ueda T, Watanabe A, Nakabayashi N. Reduced thrombogenicity of polymers having phospholipid polar groups. J Biomed Mater Res 1990;24:1069–77.
[27] Ishihara K, Ziats NP, Tierney BP, Nakabayashi N, Anderson JM. Protein adsorption from human plasma is reduced on phospholipids polymers. J Biomed Mater Res 1991;25(11):1397–407.
[28] Goda T, Konno T, Takai M, Moro T, Ishihara K. Biomimetic phosphorylcholine polymer grafting from polydimethylsiloxane surface using photo-induced polymerization. Biomaterials 2006;27(30):5151–60.
[29] Sibarani J, Takai M, Ishihara K. Surface modification on microfluidic devices with 2-methacryloyloxyethyl phosphorylcholine polymers for reducing unfavorable protein adsorption. Colloids Surf B Biointerfaces 2007;54(1):88–93.
[30] Ueda H, Watanabe J, Konno T, Takai M, Saito A, Ishihara K. Asymmetrically functional surface properties on biocompatible phospholipid polymer membrane for bioartificial kidney. J Biomed Mater Res A 2006;77(1):19–27.
[31] Abraham S, Brahim S, Ishihara K, Guiseppi-Elie A. Molecularly engineered p(HEMA)-based hydrogels for implant biochip biocompatibility. Biomaterials 2005;26(23):4767–78.
[32] Konno T, Hasuda H, Ishihara K, Ito Y. Photo-immobilization of a phospholipid polymer for surface modification. Biomaterials 2005;26(12):1381–8.
[33] Palmer RR, Lewis AL, Kirkwood LC, Rose SF, Lloyd AW, Vick TA, et al. Biological evaluation and drug delivery application of cationically modified phospholipid polymers. Biomaterials 2004;25(19):4785–96.
[34] Snyder TA, Tsukui H, Kihara S, Akimoto T, Litwak KN, Kameneva MV, et al. Preclinical biocompatibility assessment of the EVA-HEART ventricular assist device: coating comparison and platelet activation. J Biomed Mater Res A 2007;81(1):85–92.
[35] Kuiper KJ, Nordrehaug JE. Early mobilization after protamine reversal of heparin following implantation of phosphorylcholine-coated stents in totally occluded coronary arteries. Am J Cardiol 2000;85:698–702.
[36] Galli M, Sommariva L, Prati F, Zerboni S, Politi A, Bonatti R, et al. Acute and mid-term results of phosphorylcholine-coated stents in primary coronary stenting for acute myocardial infarction. Cathet Cardiovasc Intervent 2001;53:182–7.
[37] ASTM F75-01: Standard specification for cobalt-28 chromium-6 molybdenum alloy casting and casting alloy for surgical implants (UNS R30075). In: Arendt SA, Bailey SJ, editors. Annual book of ASTM standards, vol. 13, 2004.
[38] ASTM F86-04: Standard practice for surface preparation and marking of metallic surgical implants. In: Arendt SA, Bailey SJ, editors. Annual book of ASTM standards, vol. 13, 2004.
[39] Seo M, Sato N. Differential composition profiles in depth of thin anodic oxide films on iron-chromium alloy. Surf Sci 1979;86:601–9.
[40] Ishihara K, Nakabayashi N. Adhesive bone cement both to bone and metals: 4-META in MMA initiated with tri-*n*-butyl borane. J Biomed Mater Res 1989;23(12):1475–82.
[41] Yoshida K, Greener EH. Effects of coupling agents on mechanical properties of metal oxide-polymethacrylate composites. J Dent 1994;22(1):57–62.
[42] Givan DA, Fitchie JG, Anderson L, Zardiackas LD. Tensile fatigue of 4-META cement bonding three base metal alloys to enamel and comparison to other resin cements. J Prosthet Dent 1995;73(4):377–85.
[43] Bryant SJ, Nuttelman CR, Anseth KS. Cytocompatibility of UV and visible light photoinitiating systems on cultured NIH/3T3 fibroblasts in vitro. J Biomater Sci Polym Ed 2000;11(5):439–57.
[44] International Organization for Standardization 15989: Plastics—film and sheeting—measurement of water-contact angle of corona-treated films, 2004.
[45] Wang JH, Bartlett JD, Dunn AC, Small S, Willis SL, Driver MJ, et al. The use of rhodamine 6G and fluorescence microscopy in the evaluation of phospholipid-based polymeric biomaterials. J Microsc 2005;217(Pt 3):216–24.
[46] Kumar P, Oka M, Ikeuchi K, Shimizu K, Yamamuro T, Okumura H, et al. Low wear rate of UHMWPE against zirconia ceramic (Y-PSZ)

in comparison to alumina ceramic and SUS 316L alloy. J Biomed Mater Res 1991;25(7):813–28.
[47] ASTM F732-00: Standard test method for wear testing of polymeric materials used in total joint prostheses. In: Arendt SA, Bailey SJ, editors. Annual book of ASTM standards, vol. 13, 2004.
[48] International Organization for Standardization 14242-1: implants for surgery: wear of total hip-joint prostheses Part 1: loading and displacement parameters for wear-testing machines and corresponding environmental conditions for test, 2002.
[49] Suzuki T, Yuasa M, Sekine I, Yamabe H, Fujiwara T, Amano S. Investigation of the improvement of the adhesion durability of stainless steels in wet environment by surface treatment with polymer containing carboxyl groups. Shikizai 1998;71(12):746–54.
[50] Yamabe H. Stabilization of the polymer-metal interface. Progr Org Coating 1996;28:9–15.
[51] Saldivar-García AJ, Lopez HF. Microstructural effects on the wear resistance of wrought and as-cast Co–Cr–Mo–C implant alloys. J Biomed Mater Res A 2005;74(2):269–74.
[52] Sheeja D, Tay BK, Nung LN. Tribological characterization of surface modified UHMWPE against DLC-coated Co–Cr–Mo. Surf Coat Technol 2005;190(2–3):231–7.
[53] Saikko V. Wear and friction properties of prosthetic joint materials evaluated on a reciprocating pin-on-flat apparatus. Wear 1993;166(2):169–78.
[54] Ho SP, Nakabayashi N, Iwasaki Y, Boland T, LaBerge M. Frictional properties of poly(MPC-co-BMA) phospholipid polymer for catheter applications. Biomaterials 2003;24(28):5121–9.
[55] Naka MH, Morita Y, Ikeuchi K. Influence of proteoglycan contents and of tissue hydration on the frictional characteristics of articular cartilage. Proc Inst Mech Eng [H] 2005;219(3):175–82.
[56] Bell CJ, Ingham E, Fisher J. Influence of hyaluronic acid on the time-dependent friction response of articular cartilage under different conditions. Proc Inst Mech Eng [H] 2006;220(1):23–31.
[57] Iwata R, Suk-In P, Hoven VP, Takahara A, Akiyoshi K, Iwasaki Y. Control of nanobiointerfaces generated from well-defined biomimetic polymer brushes for protein and cell manipulations. Macromolecules 2004;5(6):2308–14.
[58] Yamamoto S, Ejaz M, Tsujii Y, Fukuda T. Surface interaction forces of well-defined, high-density polymer brushes studied by atomic force microscopy. 2. Effect of graft density. Macromolecules 2000;33(15):5608–12.
[59] Raviv U, Glasson S, Kampf N, Gohy JF, Jérôme R, Klein J. Lubrication by charged polymers. Nature 2003;425:163–5.

Key Engineering Materials Vols. 342-343 (2007) pp. 777-780
online at http://www.scientific.net

Prevention of Tissue Adhesion by a Spontaneously Formed Phospholipid Polymer Hydrogel

Mizuna Kimura[1], Tomohiro Konno[1], Madoka Takai[1], Noriyuki Ishiyama[2], Toru Moro[2,a] and Kazuhiko Ishihara[1,b]

[1] Department of Materials Engineering, School of Engineering, Center for NanoBio Integration

[2] Department of Orthopaedic Surgery, School of Medicine

The University of Tokyo, 7-3-1, Hongo, Bunkyo-ku, Tokyo 113-8656, Japan

[a]moro-ort@h.u-tokyo.ac.jp, [b]ishihara@mpc.t.u-tokyo.ac.jp

Keywords: Antiadhesion, Tissue healing, Hydrogel, Phospholipid polymers, Biocompatibility

Abstract. We investigated phospholipid polymer hydrogels containing Fe^{3+} ions (PMA/PMB/Fe hydrogel) for their use as antiadhesive materials in the healing tissues. These hydrogels were prepared from the aqueous solutions of poly(2-methacryloyloxyethyl phosphorylcholine (MPC)-*co*-methacrylic acid) (PMA) and poly(MPC-*co*-*n*-butyl methacrylate) (PMB). The PMA/PMB hydrogel is formed by the intermolecular interactions between PMA and PMB, and it reversibly dissociates under physiological conditions. The addition of Fe^{3+} ions could control the gelation time and the dissociation time. Mechanical properties such as the gelation time and viscoelastic properties can be controlled by the $FeCl_3$ concentration. With regard to biocompatibility, no evidence of inflammation was observed *in vivo*. Therefore, the PMA/PMB/Fe hydrogel has a potential to be used as an antiadhesive material.

Introduction

Adhesion of tissues such as a tendon and intestines after an injury or surgery is a type of inflammatory reaction. It can cause difficulty in movement or pain, thereby decreasing the quality of life of a patient [1]. Although some efforts have been invested in developing antiadhesive materials for tissues, no effective material has yet been put to practical use. The existing antiadhesive materials serve as a physical barrier to prevent contact of the healing tissue with the surrounding normal tissues. However, these materials have some drawbacks [2]: (1) The permeability of bioactive molecules such as cytokines is so low that healing is delayed. (2) Certain degree of tissue adhesion may occur after an operation for the removal of non-biodegradable materials and during adsorption of biodegradable materials.

Therefore, we propose a spontaneously formed phospholipid polymer hydrogel as a novel anti-adhesive material. This hydrogel can be prepared under physiological conditions simply by mixing the aqueous solutions containing poly(2-methacryloyloxyethyl phosphorylcholine (MPC)-*co*-methacrylic acid) (PMA) and poly(MPC-*co*-*n*-butyl methacrylate) (PMB) (Fig. 1) [3]. The hydrogel is formed by molecular interactions such as hydrogen bonding and hydrophobic interactions, and it demonstrates physical properties that correspond to the polymer structure [4,5]. Thus, it can be dissociated by changing the surrounding conditions, namely, pH, ionic strength, temperature, etc. The *in vivo* injection test did not show toxicity of the constitutive polymers—PMA and PMB. Since the PMA/PMB hydrogel has more than 95 wt% aqueous medium, it is expected to be (1) porous to allow the permeation of humoral factors, (2) biocompatible in order to prevent an inflammatory reaction, and (3) biodegradable so that a special procedure for its removal is not required after the tissues heal. The PMA/PMB hydrogel is dissociated in a large amount of aqueous medium within a few hours, and it is expected to dissociate *in vivo* within a relatively short time. Biodegradability is an advantageous property for its medical use because it can control the release of content as the degradation and eliminate the need of surgery for its removal. However, since the dissociation time of the PMA/PMB hydrogel is short, its long-term application to tissues as an antiadhesive material

is not possible. Thus, we introduced another crosslinking mechanism, that is, ionic crosslinking between counter-cation and carboxylate anion in the PMA/PMB hydrogel for achieving stabilization. Although NaCl and $CaCl_2$ did not show the expected stabilization effect, $FeCl_3$ improved the stability of the PMA/PMB hydrogel in a large amount of aqueous medium [3].

In this study, we investigated the PMA/PMB hydrogel containing $FeCl_3$ for their use as an antiadhesive material in tissues. We examined the stabilization of the PMA/PMB hydrogel by $FeCl_3$ *in vitro* and *in vivo*. We also evaluated the performance of the PMA/PMB hydrogel as an antiadhesive material *in vivo*.

Materials and Methods

Materials. The phospholipid polymers, PMA (Mn = 2.7×10^5, Mw = 8.4×10^5, and MPC mole fraction = 0.3) and PMB (Mn = 1.1×10^5, Mw = 8.6×10^5, and MPC mole fraction = 0.8), were prepared from the corresponding monomer by radical polymerization [Figure 1][6]. For this study, these polymers were supplied by the NOF Corporation (Tokyo, Japan) as 5 wt% aqueous solutions. Iron (III) hexahydrate ($FeCl_3$) was purchased from Kanto Chemical Co.

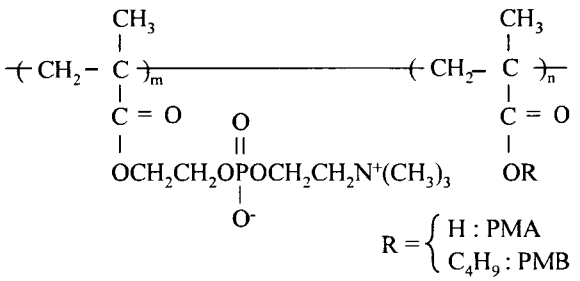

Fig. 1. Structure of PMA and PMB.

Hydrogel Preparation. Equal volumes of 5 wt% PMA and PMB aqueous solutions were taken in a microtubing and vigorously stirred for 10 s. After 10–20 s, the mixture of these MPC polymer solutions was spontaneously transformed into a hydrogel state. A hydrogel containing $FeCl_3$ (PMA/PMB/Fe hydrogel) was prepared by using PMB containing $FeCl_3$. The final concentration of $FeCl_3$ in a hydrogel is expressed by the number following the PMA/PMB/Fe hydrogel, for example, PMA/PMB/Fe hydrogel-71 implies a PMA/PMB hydrogel containing 71 mM of $FeCl_3$.

Stability of the PMA/PMB/Fe Hydrogel *in vitro and in vivo*. One gram of PMA/PMB/Fe hydrogel was put in a nylon mesh bag and immersed in 100 mL of phosphate buffered saline (PBS; 0.15 M, pH 7.1). The mesh bag was weighed at specific time intervals, and the weight of the remaining hydrogel was determined. For an *in vivo* test, a diffusion chamber (pore size, 0.3 μm) containing the PMA/PMB hydrogel or PMA/PMB/Fe hydrogel-71 was implanted subcutaneously into a mouse. After 3 weeks, the chamber was removed, and the hydrogel was observed by SEM.

Viscoelastic Properties of the Hydrogels. The aqueous solutions of PMA (0.75 mL) and PMB (0.75 mL) were injected slowly into both sides of a vibration blade (1.71 cm^2) in a liquid cell. Immediately after the injection, the blade was set in motion (vibrational amplitude, 200 μm; frequency, 20 Hz) to mix these polymer solutions in the cell in order to enable the PMA/PMB hydrogel formation. Changes in the elastic modulus (G') and the viscous modulus (G") were recorded using a rheometer (Rheolograph-Micro, Toyoseiki, Tokyo, Japan). The gelation time is defined as the time when G' becomes greater than G". The gelation time of the PMA/PMB/Fe hydrogel was also measured by using PMB containing $FeCl_3$ in the same manner. In addition, the viscoelastic properties of the hydrogel were investigated using the rheometer at a predetermined time after the hydrogel was prepared and kept at room temperature.

Results and Discussion

Fig. 2 shows the effect of $FeCl_3$ addition on the stability of the PMA/PMB/Fe hydrogel. The relative weight of PMA/PMB/Fe hydrogel-14 gradually decreased, and it completely dissociated within 6 h after its immersion in PBS. PMA/PMB/Fe hydrogel-28 also dissociated completely within 24 h, although PMA/PMB/Fe hydrogel-39 and PMA/PMB/Fe hydrogel-71 retained almost a constant weight after a slight initial decrease. Because a Fe^{3+} ion theoretically interacts with 3 carboxylate anions, the residual carboxylic acid groups exist in PMA/PMB/Fe hydrogel-14 and PMA/PMB/Fe hydrogel-28. The $FeCl_3$ concentration is adjusted to the theoretical ratio in

PMA/PMB/Fe hydrogel-39. Thus, PMA/PMB/Fe hydrogel-39 and PMA/PMB/Fe hydrogel-71 did not dissociate because of the higher $FeCl_3$ concentration.

The relative weight of PMA/PMB/Fe hydrogel-28 showed a slight initial increase, and then it steadily decreased. This suggests swelling of the hydrogel immediately after its immersion in PBS, followed by its dissociation. When the PMA/PMB/Fe hydrogel is immersed in PBS, swelling of the hydrogel and diffusion of $FeCl_3$ starts. Influx of water can cause ionization of the carboxylic acid groups and lead to electrostatic repulsion between the carboxylate anions. As a result, the polymer concentration and the crosslinking density decreases. Subsequently, the polymer networks collapse, i.e., dissociation of the hydrogel occurs. As seen in the yellowish PBS obtained after the immersion of the hydrogel, diffusion of the Fe^{3+} ions and swelling of PMA/PMB/Fe hydrogel-71 and PMA/PMB/Fe hydrogel-39 is possible. However, even during the swelling process, these hydrogels retained the polymer network and attained equilibrium due to a high density of Fe^{3+} crosslinking.

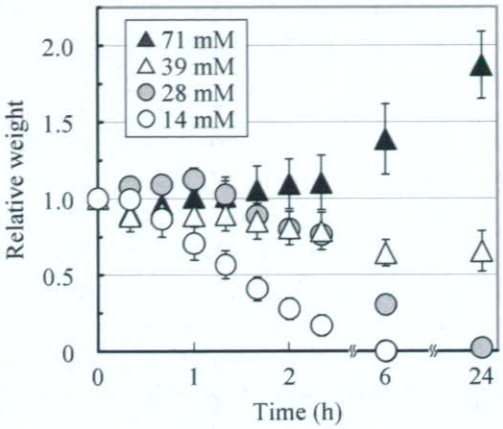

Fig. 2 Change in the weight of PMA/PMB hydrogel containing $FeCl_3$ immersed in PBS.

Although PMA/PMB/Fe hydrogel-71 was implanted subcutaneously, stabilization of the PMA/PMB hydrogel containing Fe^{3+} was observed. That is, while the PMA/PMB hydrogel was dissociating, PMA/PMB/Fe hydrogel-71 remained and maintained the hydrogel state even after 3 weeks. A three-dimensional network structure could be observed under SEM, and the results of viscoelastic measurements also indicated the defining characteristic of a hydrogel, that is, G' > G".

Table 1 shows the gelation time of the PMA/PMB hydrogel and the PMA/PMB/Fe hydrogel. The gelation time was longer for the PMA/PMB hydrogel than for the PMA/PMB/Fe hydrogel. Since the $FeCl_3$ solution has a low pH, ionization of the carboxylic acid groups in PMA can be suppressed by mixing PMA with PMB containing $FeCl_3$. Suppression of the carboxylic acid groups leads to hydrogen bond formation, resulting in the shortening of the gelation time of the PMA/PMB/Fe hydrogel when compared with that of the PMA/PMB hydrogel. Increase in the $FeCl_3$ concentration decreased the gelation time. This is because the pH of PMA/PMB/Fe hydrogel-142 was lower than that of PMA/PMB/Fe hydrogel-71.

Table 1 Gelation time of PMA/PMB hydrogel containing $FeCl_3$

	Gelation time (s)
PMA/PMB hydrogel	1007 ± 137
PMA/PMB/Fe hydrogel-71	605 ± 101
PMA/PMB/Fe hydrogel-142	468 ± 47

Thus, the addition of $FeCl_3$ significantly reduced the gelation time and the dissociation time of the PMA/PMB/Fe hydrogel; moreover, these parameters can be controlled by the $FeCl_3$ concentration.

The viscoelastic properties of the PMA/PMB hydrogel and the PMA/PMB/Fe hydrogel are shown in Fig. 3. With regard to the gelation time, agitation efficiency was so high that it took shorter time compared to the preparation method described in the gelation time measurement section. Vigorous stirring by a vortex mixer for 10 s is sufficient to prepare both PMA/PMB and PMA/PMB/Fe hydrogels. The mechanical strength of the PMA/PMB/Fe hydrogel immediately after its preparation (10 s) was so low that it appeared almost sol. Both G' and G" of PMA/PMB/Fe hydrogel-142 were lower than those of PMA/PMB/Fe hydrogel-71. G' and G" of the

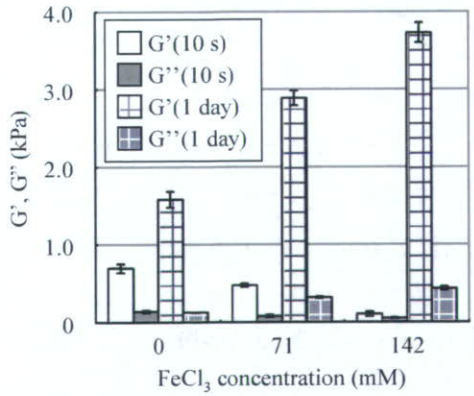

Fig. 3 Change in the elastic modulus (G') and the viscous modulus (G") of PMA/PMB hydrogel containing $FeCl_3$.

PMA/PMB hydrogel were higher than those of the PMA/PMB/Fe hydrogel. One day after the hydrogel preparation, increase in G' and G" was observed in all the hydrogels; G' of the PMA/PMB hydrogel was more than double its value immediately after the hydrogel preparation, while G" remained almost constant. It is noteworthy that G' of PMA/PMB/Fe hydrogel-71 increased 6-fold and that of PMA/PMB/Fe hydrogel-142 increased more than 60-fold after 1 day. G" of PMA/PMB/Fe hydrogel-71 also increased by approximately 4-fold and that of PMA/PMB/Fe hydrogel-142 increased more than 8-fold. Interestingly, among the 3 hydrogels, G' of PMA/PMB/Fe hydrogel-142 was the lowest immediately after the hydrogel preparation, but it was the highest after 1 day; this observation can be explained by the ionic crosslink formation.

During clinical application, the treated tissue will be covered by an antiadhesive agent and then sutured. Thus, the change in the mechanical properties during and after surgery would determine the clinical usefulness of an antiadhesive agent. A point worth noting is that immediately after its preparation, the PMA/PMB/Fe hydrogel is a weak gel; however, it improves its mechanical strength with time. This change in the mechanical properties of the PMA/PMB/Fe hydrogel can enable the hydrogel to attain a specific shape according to the application site and solidify after suturing; these features are a requisite for an antiadhesive material.

Furthermore, implantable antiadhesive materials should also be biocompatible in order to prevent the occurrence of any inflammatory reaction that would result in adhesions. Based on the results of the *in vivo* injection test, we have previously reported that PMA and PMB do not show notable adverse effects [5]. Although $FeCl_3$ is applied to dental materials to facilitate the adhesion of dental prosthesis to the dentin tissue, a report has shown the potential of $FeCl_3$ to cause oxidative stress on cells leading to the development of mutation [7]. The biocompatibility of the PMA/PMB/Fe hydrogel should be closely examined. We have been investigating the antiadhesive property of hydrogels and its effect on healing. No evidence of inflammation was observed in the tissues surrounding the hydrogel. We shall provide detailed reports of the results elsewhere.

Conclusions

A PMA/PMB hydrogel containing $FeCl_3$ (PMA/PMB/Fe hydrogel) shows that the mechanical properties of a hydrogel can be controlled by a combination of hydrogen bonding and ionic crosslinking. Severe inflammatory reaction was not observed in the tissues surrounding the hydrogel. Therefore, it can be concluded that the PMA/PMB/Fe hydrogel satisfies the basic requirements for an antiadhesive material.

Acknowledgement

This study was financially supported by a Grant-in-Aid for Scientific Research (B) (No. 17300144).

References

[1] C.L. Zhang, W.M. Tian and F.Z. Cui: Curr. Appl. Phys. 5 (2005), p. 411

[2] J. H. Lee, A.K. Go, S.H. Oh, K.E. Lee and S.H. Yuk: Biomaterials 26 (2005), p. 671

[3] M. Kimura, K. Fukumoto, J. Watanabe, and K. Ishihara: J. Biomater. Sci. Polym. Edn. 15 (2004), p. 631

[4] M. Kimura, K. Fukumoto, J. Watanabe, M. Takai and K. Ishihara: Biomaterials 26 (2005), p. 6853.

[5] M. Kimura, M. Takai and K. Ishihara: J. Biomed. Mater. Res. (2006), in press.

[6] K. Ishihara, T. Ueda, and N. Nakabayashi, Polym. J. 22 (1990), p. 355.

[7] S. Toyokuni: Free Radic. Biol. Med. 20 (1996), p. 553

J Mater Sci: Mater Med (2007) 18:1809–1815
DOI 10.1007/s10856-007-3063-0

Effects of photo-induced graft polymerization of 2-methacryloyloxyethyl phosphorylcholine on physical properties of cross-linked polyethylene in artificial hip joints

Masayuki Kyomoto · Toru Moro · Tomohiro Konno · Hiroaki Takadama · Hiroshi Kawaguchi · Yoshio Takatori · Kozo Nakamura · Noboru Yamawaki · Kazuhiko Ishihara

Received: 15 March 2006 / Accepted: 31 May 2006 / Published online: 5 May 2007

Abstract Osteolysis caused by wear particles from polyethylene in the artificial hip joints is a serious issue. We have used photo-induced radical graft polymerization to graft 2-methacryloyloxyethyl phosphorylcholine (MPC) polymer onto the surface of cross-linked polyethylene (CLPE-*g*-MPC) in order to reduce friction and wear at the bearing surface of the joint. The physical and mechanical properties of CLPE and CLPE-*g*-MPC were not significantly different, expect that the friction coefficient of untreated CLPE cups was 0.0075, compared with 0.0009 for CLPE-*g*-MPC cup, an 88% reduction. After 3.0×10^6 cycles in the hip joint simulator test, we could not observe any wear of CLPE-*g*-MPC cups. We concluded that the advantage of photo-induced radical graft polymerization technique was that the grafted MPC polymer gave a high lubricity only on the surface and has no effect on the bulk properties of the CLPE substrate.

M. Kyomoto (✉) · N. Yamawaki
Research and Development Corporate Division, Japan Medical Materials Corporation, Uemura Nissei Bldg. 9F, 3-3-31 Miyahara, Yodogawa-ku, Osaka 532-0003, Japan
e-mail: kyomotom@jmmc.jp

T. Moro · H. Kawaguchi · Y. Takatori · K. Nakamura
Department of Orthopaedic Surgery, School of Medicine, The University of Tokyo, Tokyo, Japan

T. Konno · K. Ishihara
Department of Materials Engineering, School of Engineering and Center for NanoBio Integration, The University of Tokyo, Tokyo, Japan

H. Takadama
Materials Research and Development Laboratory, Japan Fine Ceramics Center, Atsuta-ku, Nagoya, Japan

Introduction

The most widely used bearing couple for artificial joint systems is the combination of an ultra-high molecular weight polyethylene (UHMWPE) acetabular component and a Co–Cr–Mo alloy femoral component. However, osteolysis caused by wear particles of UHMWPE has emerged as a serious issue [1–3]. Decreasing the number of wear particles from UHMWPE is one way to prevent osteolysis, and different combinations of bearing surfaces and improvements in the bearing materials themselves have been focused. Several highly cross-linked polyethylenes (CLPE) irradiated with 50–105 kGy have been launched since 1998, and they have been used extensively [4]. Gamma-ray and electron beam irradiation at various doses are used by many manufacturers to produce CLPE. In published reports, CLPE produced with 50–105 kGy irradiation shows an 80–90% reduction in wear rate compared with conventional polyethylene [5, 6]. Clinical results have confirmed the excellent anti-wear properties of CLPE. While the efficacy of CLPE is attested by many reports [7–11], the in vivo reduction of wear is only a decrease of 40–60%, so further improvement is desired.

We have recently developed a new-concept artificial hip joint system with 2-methacryloyloxyethyl phosphorylcholine (MPC) polymer grafted onto the surface of CLPE (CLPE-*g*-MPC), aiming to reduce wear and avoid bone resorption [12]. MPC is a methacrylate monomer which has a phospholipid polar group in a side chain, and which is used to make new concept biomaterials as designed by Ishihara et al. [13], who were inspired by the neutral phospholipids of biomembranes. Many polymers consisting MPC unit are widely used as biomaterials [14, 15]. Various medical devices using MPC polymer have already been developed and clinically used with the approval of the